Bioresource Technology Reports 27 (2024) 101909

Contents lists available at ScienceDirect

Bioresource Technology Reports

journal homepage: www.sciencedirect.com/journal/bioresource-technology-reports

Thermal responses of *Tetradesmus obliquus* for industrial outdoor cultivation

Hidehiko Kato [a,*], Hirono Suzuki [a], René H. Wijffels [c], Peter S.C. Schulze [a,b], Chris J. Hulatt [a]

[a] Faculty of Bioscience and Aquaculture, Nord University, Bodø, Norway
[b] GreenCoLab—Associação Oceano Verde, Algarve University, 8005-139 Faro, Portugal
[c] Wageningen University & Research (WUR), Wageningen, Netherlands

ARTICLE INFO

Keywords:
Tetradesmus obliquus
Thermal performance
Gene expression
UTEX393
Turbidostat
Photobioreactor

ABSTRACT

In microalgae cultivation systems, fluctuating temperatures impact growth rates and biomass quality, whilst extremes of temperature can lead to the loss of large-scale cultures. Evaluation and selection of strains based on their performance under different temperatures could offer substantial improvements by reducing costs and increasing yields. Here the thermal performance of *Tetradesmus obliquus* UTEX393 was compared with a novel isolate of the same species, SNS0120, using turbidity-controlled flat-panel photobioreactors. UTEX393 showed higher growth performance at all temperatures and a higher thermal limit compared to SNS0120. Total fatty-acids were not influenced by temperature, but the fatty-acid profiles varied, and omega-3/6 ratios were lower under high temperatures. Transcriptomic analysis of UTEX393 showed that temperature caused substantial shifts in gene expression, with 4971 significantly differentially expressed genes during a temperature upshift from 10 °C (low temperature) to 25 °C (optimal temperature), and 3683 genes significantly differentially expressed from 25 °C (optimal temperature) to 34 °C (high temperature).

1. Introduction

Microalgae are increasingly cultivated in large-scale outdoor photobioreactors (PBRs) and raceway ponds for the production of food, feed products, and wastewater bioremediation (Erbland et al., 2020; Patnaik et al., 2019; Plöhn et al., 2021). However, scaling up cultures outdoors brings challenges in the management of culture conditions, especially variations in light and temperature. Throughout the day, ponds and PBRs in particular experience substantial fluctuations in temperature that impact their productivity (Barten et al., 2021; Slegers et al., 2013). For example, without expensive cooling systems, photobioreactors in hot climates may reach nearly 50 °C, substantially higher than the optimal growth temperature (20 to 35 °C) of most commercially valuable microalgae species (Bleeke et al., 2014; Ras et al., 2013). Because temperature directly controls the yield of photobioreactors, it is a major variable affecting both the cost and energetic efficiency of producing algal commodities at scale (Gifuni et al., 2019; Handler et al., 2014; Ubando et al., 2022). Evaluation of the thermal tolerance of production strains could therefore offer significant improvements in the yields of large-scale outdoor cultivations (Lage et al., 2021).

Microorganisms in general show an approximately exponential increase in metabolic rate with temperature (Huete-Stauffer et al., 2015; Padfield et al., 2015; Schulte, 2015). Although the effect of temperature is typically weaker on photosynthetic organisms, it remains a major variable driving productivity, perhaps by two or three-fold, over the physiological tolerance range of an alga(Padfield et al., 2017). Whilst low temperatures can limit productivity, high temperatures above a thermal optimum can lead to cell death and the collapse of cultures, which has serious consequences for the industrial production of algae (Barten et al., 2021; Casagli and Bernard, 2022). A narrow range between the thermal optimum and the upper threshold temperature indicates strains are sensitive to temperature fluctuation, while a wider thermal range indicates more robust strains (Ras et al., 2013). Microalgae are also predisposed to adapt to new thermal environments (Cheregi et al., 2021; Huertas et al., 2011), ranging from short-term responses driven by gene expression (Millington et al., 2019) to long-term evolutionary adaptations (Yvon-Durocher et al., 2017).

A variety of bioreactor and pond designs have been developed that vary in thermal performance, including their heat exchange properties, thermal inertia (heat capacity), and use of active temperature control (Huang et al., 2017). However, phototrophic organisms ultimately require cultivation systems with a high surface area to volume ratio for accessing sunlight, which generally makes PBRs and ponds sensitive to changes in ambient temperature and light absorbance. As a result,

* Corresponding author at: Faculty of Biosciences and Aquaculture, Nord University, Bodo, Norway.
E-mail address: hidehiko.kato@nord.no (H. Kato).

https://doi.org/10.1016/j.biteb.2024.101909
Received 25 April 2024; Received in revised form 30 June 2024; Accepted 15 July 2024
Available online 18 July 2024

temperatures inside bioreactors naturally vary based on geographic location, seasonal and daily weather patterns, bioreactor/pond system design, and potentially long-term climate change (Barten et al., 2021; Béchet et al., 2013).

In addition to the growth rate, temperature also affects biomass quality including the lipid composition of the cells. For instance, *Tetradesmus obliquus* UTEX393 is known to alter its cellular lipid content in response to changes in temperature, pH, and nutrient supply (Breuer et al., 2012). *T. obliquus* UTEX393 cells, which measure approximately 5 to 8 μm in length, can tolerate temperatures from approximately 10 °C to 39 °C depending on salinity and nutrient supply (Huesemann et al., 2023), and can accumulate lipids of around 30 to 40 % dry mass under nitrogen-starved conditions (Calhoun et al., 2021; Shao et al., 2017). However, identifying the sole effect of temperature on total lipid composition and the fatty-acid profile requires highly controlled experimental bioreactor conditions, to isolate the effect of temperature from other cultivation variables such as nutrient supply and light intensity.

At the molecular level, temperature alters the expression of metabolic pathways and may even inactivate enzymes performing key metabolic functions (Flynn et al., 2010; Shekh et al., 2022). Although temperature can alter the expression of thousands of different genes (Lin et al., 2022; van der Knaap and Verrijzer, 2016), processes including photosynthesis, respiration, protein synthesis, and lipid metabolism are perhaps the most significant for their impact on microalgal industrial bioprocesses in bioreactors, because they relate to growth, gas exchange, elemental stoichiometry and the biochemical profile of the microalgal cell. Transcriptomics provides a comprehensive analysis of genome-wide metabolic regulation (Hulatt et al., 2020; Milward et al., 2016; Yadav et al., 2018), although analysis of thermal effects on the transcriptome has not been studied in *Tetradesmus* and more widely there is limited relevant data for microalgae cultivated in industrial bioreactor systems.

The objective of this work was to test the effects of temperature on the performance of two *Tetradesmus* strains intended for outdoor mass cultivation by studying the growth rate, fatty acid composition, and photosynthetic performance. The molecular and metabolic dynamics that underpin responses to temperature, the effects of low, optimal, and high temperature on strain UTEX393 were also compared using genome-wide gene expression.

2. Materials and methods

2.1. Tetradesmus strains, identification and cultivation

Tetradesmus obliquus UTEX393 was originally supplied by UTEX Culture Collection of Algae (USA, https://utex.org). Strain SNS0120 was obtained from NECTON Companhia Portuguesa de Culturas Marinhas SA. SNS0120 was isolated from freshwater in Pataias, Portugal (39.6832°N, 9.0018°W) and selected as one of the strain candidates for the AlgaCycle project (EEA and Norway grants) for large-scale production of aquafeed ingredients. Species identification of SNS0120 was conducted with internal transcribed spacer 2 (ITS2) ribosomal DNA (rDNA) sequences for high taxonomic resolution. DNA extraction was performed using an E.Z.N.A.® HP Plant DNA Kit (Omega Bio-tek, Georgia, USA). Bead milling (6000 rpm for 5 min, Precellys evolution homogenizer, Bertin Technologies, Montigny-le-Bretonneux, France) with 0.1 mm glass beads were used for cell lysis. DNA quantity and quality were checked with a NanoDrop® (ThermoFisher Scientific, MI, USA). PCR amplification and sequencing were performed by Macrogen using forward (ITS3: 5'-GCATCGATGAAGAACGCAGC-3′) and reverse (ITS4: 5'-TCCTCCGCTTATTGATATGC-3′) primers. ITS2 rDNA sequences of species in the genus *Tetradesmus* were acquired from NCBI for phylogenetic analysis (Wynne and Hallan, 2015). The ITS2 rDNA sequences were aligned with MUSCLE (Multiple sequence comparison by log-expectation) and trimmed to the same length (253 bp) in MEGAX v10.1.8 (Kumar et al., 2018). The phylogenetic tree was constructed by using the maximum likelihood method with the K2 + G model and 1000 bootstrap replications.

Growth media was Bold's basal medium (BBM) (Bischoff and Bold, 1963) modified with triple nitrate formulation (3 N-BBM) and supplied at triple concentration (effectively 3 × 3N-BBM) to ensure that nutrient deprivation could not occur in high cell density bioreactors. The 3 × 3N-BBM consisted of $NaNO_3$ 27 mM, $MgSO_4{\cdot}7H_2O$ 0.9 mM, NaCl 0.4 mM, K_2HPO_4 2.6 mM, KH_2PO_4 7.7 mM, $CaCl_2{\cdot}2H_2O$ 0.5 mM, $ZnSO_4{\cdot}7H_2O$ 0.09 mM, $MnCl_2{\cdot}4H_2O$ 0.02 mM, MoO_3 0.01 mM, $CuSO_4{\cdot}5H_2O$ 0.02 mM, $Co(NO_3)_2{\cdot}6H_2O$ 0.01 mM, H_3BO_3 0.6 mM, $Na_2EDTA{\cdot}2H_2O$ (Titriplex III) 0.4 mM, KOH 1.7 mM, $FeSO_4{\cdot}7H_2O$ 0.05 mM, soil extract 50 mL/L, Thiamine (vitamin B_1) 3 μM, Biotin (vitamin H) 1.02 nM, and Cyanocobalamin (vitamin B_{12}) 0.1 nM. The medium was adjusted to pH 6.5, filtered with glass microfiber filters (47 mm diameter x 0.7 mm thickness, pore size approximately 1 μm, VWR), and autoclaved (121 °C for 20 min) prior to use. Cultures of UTEX393 and SNS0120 were prepared in 400 mL tube photobioreactors at 10 °C, the experimental starting temperature, under constant light at 70 μmol $m^{-2}{\cdot}s^{-1}$ photosynthetically active radiation (PAR) in a Series 6000 incubator (Termaks AS, Bergen Norway). Atmospheric air was used for maintaining the culture without additional CO_2 enrichment.

2.2. Experimental photobioreactor systems

The experimental photobioreactors were Algaemist-S flat-plate systems (Wageningen University, The Netherlands) of 400 mL volume with an airlift loop configuration (Fig. 1). This PBR is a small-scale model system of the much larger flat-panel PBRs that are commonly used for industrial production. The temperature of the cultivation vessel was controlled at ±0.1 °C by a water jacket supplied by a recirculating heater/cooler (A25, Thermo Fisher Scientific). The cultivation vessel had a 14 mm light path with aeration provided by a mixture of filtered air at 200 ± 4 mL/min and CO_2 at 4 ± 1 mL/min (2 % CO_2 in air). The initial temperature was set to 10 °C and the incident light intensity was 140 μmol $m^{-2}{\cdot}s^{-1}$ PAR supplied by warm-white LEDs (Bridgelux, BXRA W1200) throughout the experiments. The incident light intensity was determined by the average irradiance over the surface of the inside of the front glass panel of the reactor by an LI-250A light meter (LI-COR Biosciences, USA). Using turbidostat control, the medium was automatically added to keep the turbidity of the culture constant. The

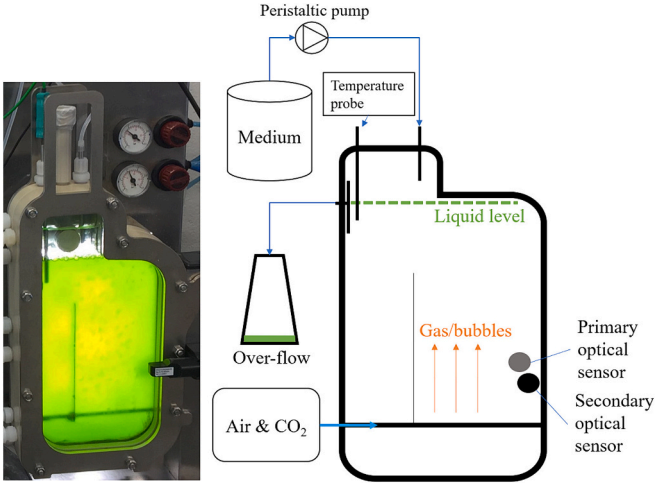

Fig. 1. The assembled 400 mL Algaemist-S flat-panel photobioreactor. The flask indicated as "over-flow" in the diagram collects the outflow from the reactor, which was recorded daily. The secondary optical sensor continuously measures the transmitted light, which controls the turbidity by adding fresh cultivation medium by activating a peristaltic pump. Light-blocking covers were temporarily removed in this picture.

volume of the out-flow was measured every 24 h. The temperature experiment was initiated after the volume of the out-flow became approximately constant. Temperatures tested for the experiment were 10, 13, 16, 19, 22, 25, 28, 31, 34, 37, and 40 °C. The experiment was duplicated for strain SNS0120 and quadruplicated for the UTEX393. The additional replicates for UTEX393 were included to ensure robust statistical power in the subsequent RNA-seq gene expression analysis experiment of this strain. Photobioreactor units were alternated for each strain in order to avoid any small statistical biases arising from e.g. instrument-specific effects.

2.3. Growth rate measurement

Both UTEX393 and SNS0120 were exposed to each temperature, starting at 10 °C and incremented by 3 °C every three days until the cultures collapsed at high temperatures. Growth was determined by the average out-flow volume measured on the second and the third day at the set temperature. At constant cell density under turbidity control, the growth rate was determined according to Eq. (1):

$$\textit{Growth rate}\ \left(d^{-1}\right) = \frac{V_{out}}{V_t} \tag{1}$$

Where V_{out} is the bioreactor out-flow volumes per day ($mL{\cdot}d^{-1}$) measured at constant optical density at each set temperature, and V_t is the total volume of the photobioreactor (400 mL).

2.4. Sampling

At the end of each temperature treatment, samples were collected using sterile syringes for lipid analysis, transcriptomic analysis, photosynthesis measurements, optical density measurement, and dry weight measurements. For the lipid analysis, 10 mL of culture was added to a 15 mL centrifuge tube and spun for 3 min at 1110 rcf. The supernatant was discarded, and the biomass was transferred into a 1.5 mL microfuge tube with 1 mL of Milli-Q water and then centrifuged for 1 min. The supernatant was removed and the microfuge tube containing the pellet was immediately dipped into liquid nitrogen and then stored at −80 °C. For transcriptomic analysis, 1.5 mL of sample was collected into 1.5 mL microfuge tubes. The samples were pelleted by centrifugation (4470 rcf for 2 mins), the supernatant was discarded, then the cell pellets were immediately frozen in liquid nitrogen and stored at −80 °C until RNA extraction.

2.5. Dry weight and optical density measurement

For optical density measurement, 150 µL of the sample was added to a 1 cm path length cuvette and diluted 6-fold by adding 750 µL of Milli-Q water. The optical density at 540 nm and 680 nm was measured with a spectrophotometer DR3900 (HACH, Manchester, UK). Dry weight was measured by vacuum filtering a defined volume of culture through pre-weighted glass microfiber filters (47 mm diameter, pore size 1.0 µm, VWR). The filter and the algal biomass were washed with Milli-Q filtered water and dried overnight at 97 °C, then re-weighed with a precision balance XA204DR (Mettler Toledo, Greifensee, Switzerland) to determine the algal mass on the filter.

2.6. Maximum photochemical efficiency of PSII and electron transport rate

Immediately after sampling, 10 µL of cell culture was diluted with 1250 µL of Mill-Q water in a quartz cuvette (1 cm path length), which was placed in a Multi-Color PAM chlorophyll fluorometer (Heinz Walz GmbH, Germany) and dark-adapted for 5 mins. Following dark-adaptation, a saturation pulse measurement using blue (440 nm) light was applied to measure the maximum quantum yield of photosystem II (F_v/F_m) (Kitajima and Butler, 1975) described in Eq. (2):

$$\frac{F_m - F_0}{F_m} = \frac{F_v}{F_m} \tag{2}$$

Where F_0 is the minimal fluorescence under modulated measuring light, F_m is the maximum fluorescence under saturating light, and the difference between these two values was the variable fluorescence (F_v). The saturation pulse measurement was extended to a full rapid light curve protocol where the sample was sequentially exposed to increasing actinic illumination with 20 s intervals between the steps, and the relative electron transport rate (*rETR*) was calculated at each step according to Eq. (3):

$$rETR = PAR \times ETR_{Factor} \times Y(II) \tag{3}$$

Where ETR_{Factor} was the default setting for the relative absorbance of photosystem II (0.42). The effective photochemical yield of photosystem II ($Y(II)$) (Genty et al., 1989) was calculated according to Eq. (4):

$$Y(II) = \frac{F_m{}' - F}{F_m{}'} \tag{4}$$

Where $F_m{}'$ is the maximum fluorescence of the illuminated sample during the saturation pulse and F is the fluorescence level immediately before the saturation pulse. The light curve was fitted with the Platt model to estimate the maximum *rETR*, or $rETR_{max}$ (Platt et al., 1980).

2.7. Fatty acid analysis

Fatty acid extraction and quantification was performed as described by Breuer et al. (2012) and Suzuki et al. (2019). Samples were lyophilized in a FreeZone −50 °C freeze dryer (Labconco Corporation, USA) for 48 h. Approximately 6 mg of lyophilized samples were weighed with a precision balance (Mettler Toledo MX-5, USA) and transferred into 2 mL bead-beating tubes containing 400 µL of 0.1 mm glass beads. 1 mL of chloroform: methanol (4:5) mixture was added to each tube, and then cell disruption was performed with a Precellys evolution homogenizer (Bertin Instruments, France) at 6000 rpm, 60 s for 3 cycles with 30-second intervals. The homogenate was transferred to a 10 mL glass tube with the addition of another 3 mL chloroform: methanol (4:5) mixture. Phase separation was performed by adding 2.5 mL of 50 mM Tris-base solution (2-Amino-2-(hydroxymethyl)-1,3-propanediol including 1 M NaCl and pH adjusted to 7.5 with HCl) to the glass tubes followed by centrifugation (180 rcf, 5 min, Hettich Universal 320R). The chloroform fraction (bottom phase) was transferred to the fresh 10 mL glass tubes and solvent evaporated under a stream of N_2 gas to recover total lipids using Reacti-Therm Heating and Stirring Modules TS-18820 (Thermo Scientific). Lipids were derivatized to fatty acid methyl esters (FAMEs) by adding 3 mL of methanol containing 5 % H_2SO_4 followed by 3 h of incubation at 70 °C in an oven (DRY-Line, VWR). Aliquots of 3 mL of H_2O followed by 3 mL of hexane were added to the FAMEs, and then 15 min of vortex-mixing followed by centrifugation (180 rcf, 5 min). Quantification of the FAMEs in the hexane fraction was conducted with a Gas Chromatograph and Flame Ionization Detector (GC-FID, SCION 436-GC, SCION Instruments) fitted with a splitless injector and a 30 m CP-WAX column (Agilent Technologies, USA). Supelco 37-component standards (Sigma-Aldrich, Oslo, Norway) were used for the identification and quantitation of the FAMEs with five-point calibrations. Blanks were included throughout extraction and derivatization to eliminate trace background peaks.

2.8. Transcriptomic analysis

Samples of strain UTEX393 were placed on ice and 500 µL of Trizol (Sigma-Aldrich, Oslo, Norway) was added to each, then gently mixed by pipette and transferred to 2 mL tubes containing 0.3 mL of glass beads

(0.1 mm). Cells were homogenized with a Precellys evolution homogenizer (Bertin Technologies, Montigny-le-Bretonneux, France) at 6000 rpm for 2 cycles of 60 s with 10-second intervals. The homogenized samples were incubated for 5 min at room temperature, then 200 μL of chloroform was added followed by 5 s of vortex-mixing and 3 mins incubation at room temperature. Samples were centrifuged (12,000 rcf, 15 min, 4 °C) and 100 μL of the supernatant containing RNA was transferred to a 1.5 mL Eppendorf tube followed by 100 μL of 100 % ethanol. The mixture was transferred to a Zymo RNA clean and concentrator spin column (Zymo Research, USA), and the kit instructions were followed. Clean RNA was eluted in molecular grade water and quality-checked with a NanoDrop One® (ThermoFisher Scientific, MI, USA) and TapeStation 2200 with RNA ScreenTape (Agilent Technologies, Waldbronn,Germany) to determine RNA quantity and quality with RNA integrity RIN >6.3.

Library preparation and sequencing were performed by NovoGene Corporation (UK) using 150 bp PE sequencing on an Illumina HiSeq X instrument. Four replicate samples each from temperatures 10 °C, 25 °C, and 34 °C generated 64,522,342 to 89,497,194 reads each. Adaptor sequences were trimmed from raw reads, and the raw reads which contain N (undetermined base) >10 % or low-quality bases (Qscore ≤ 5) >50 % bases, were filtered. Raw reads were submitted to NCBI Sequence Read Archive (SRA) under the accession number PRJNA870074.

The *T. obliquus* UTEX393 reference genome sequence (GCA_900108755.1_sob1_genomic.fna) was obtained from NCBI. We were unable to obtain a gene annotation file, therefore the genome sequence was annotated *de novo* using the transcript sequences generated in this study as described in Hulatt et al. (2021). Briefly, a *de novo* library of repetitive elements was constructed using RepeatModeler, which was used to annotate and mask repeat elements in the genome sequence. Genes were then annotated using Braker1 and RNA-seq evidence from three sample libraries (one each from 10 °C, 25 °C, and 34 °C treatments) (Hoff et al., 2016). In total 16,432 protein-coding genes were annotated with the BUSCO completeness score of 96.4 % against the Chlorophyta_odb10 reference. Full BUSCO results and a summary of repeat elements are shown in Supplemental data 1 and Supplemental data 2. Annotation of gene function was conducted using BlastP against the SwissProt database, plus InterProScan and EggNog mapping tools to provide ontology support and pathway mapping.

Mapping of RNA-seq reads to the genome was conducted with HISAT2 with the paired reads option (Zhang et al., 2021). Aligned reads were assigned to genomic CDS features and counted using the "featureCounts" function in the SUBREAD program (Liao et al., 2014). Feature read counts for all 12 samples were analyzed using R version 4.1.2. Differentially expressed genes were determined using "edgeR", "limma", and "variancePartition" R packages (Hoffman and Roussos, 2021; Hoffman and Schadt, 2016; Law et al., 2014). Due to the repeated measurements at increasing temperatures, we included a random experimental-unit effect in the design matrix. The *voomWithDreamWeights()* R-function was applied to calculate log2-counts per million (logCPM), estimate the mean-variance relationship, and to compute appropriate observation-level weights. The *dream()* R-function was used to fit the linear mixed model (restricted maximum likelihood, REML) for each gene, calculating the log2-Fold Change. The Kenward-Roger approximation and the Satterthwaite approximation were used to estimate the *p*-values and control the false positive rate (Gabriel, 2020). GO enrichment analysis was performed separately for up- and down-regulated genes using classic Fisher's exact test in R-package topGO v2.46 (Alexa and Rahnenfuhrer, 2021) (Supplemental data 7). Supplemental data 8 presents the differentially expressed genes, including only those for which annotations were possible.

2.9. Statistical analysis

Pairwise *t*-tests were conducted on the UTEX393 dataset to determine whether there were any significant differences in growth rate, photosynthesis, and lipid contents between low (10 °C) and optimal (25 °C) temperature; or between optimal (25 °C) and high (34 °C) temperatures. The *pairwise.t.test()* in R was applied, and the Shapiro-Wilk *shapiro.test()* was used to confirm that the data were approximately normally distributed. No statistical test was performed for strain SNS0120.

Thermal performance curves were fitted using the rTPC and the nls.multstart R-packages (Padfield et al., 2021). A total of 24 thermal performance models (Supplemental data 3) were fitted to the growth rate data and model performance was compared using Akaike's information criterion (AICc) (Angilletta, 2006; Boatman et al., 2017; Briere et al., 1999; Hinshelwood, 1946; DeLong et al., 2017; Flinn, 1991; Jöhnk et al., 2008; Johnson and Lewin, 1946; Kamykowski, 1985; Kontopoulos et al., 2018; Lactin et al., 1995; Lynch and Gabriel, 1987; Montagnes et al., 2008; Niehaus et al., 2012; O'Neill et al., 1972; Ratkowsky et al., 1983; Rezende and Bozinovic, 2019; Schoolfield et al., 1981; Spain, 1982; Thomas et al., 2017; Weibull, 1995). After the best-fit model (model with the lowest AICc) was determined, the area under the curves was calculated using the function *auc()* in the Flux R-package in order to summarize the differences between the two strains.

3. Results

3.1. Phylogenetic analysis

Strains UTEX393 and SNS0120 differed by 2 bp between their ITS2 rDNA sequences, which is typically amongst the most variable of the popular genetic markers and thus most sensitive to species differentiation. Phylogenetic comparison amongst other strains of the genus *Scenedesmus/ Tetradesmus* confirmed that UTEX393 and SNS0120 were closely related strains of the same species (Fig. 2).

3.2. Growth rate and thermal performance of UTEX393 and SNS0120

The growth rate of both UTEX393 and SNS0120 increased with increasing temperature from 10 to 25 °C (Fig. 3, Supplemental data 4). Strain UTEX393 reached a growth rate of 0.99 ± 0.05 d^{-1} at 25 °C, whilst the growth rate of SNS0120 reached only 0.75 ± 0.01 d^{-1}. At higher temperatures, both strains showed reduced growth and at 31 °C SNS0120 cultures became pale yellow and flocculated within 24 h. The SNS0120 culture collapsed shortly after, and higher temperatures were not tested for this strain. In contrast, UTEX393 showed strong growth until 37 °C, indicating a wider thermal tolerance range than SNS0120. At 40 °C, UTEX393 cultures finally collapsed.

A total of 22 different thermal performance curve models were fitted to the growth rate data, and the best-fitting models were determined for both UTEX393 and SNS0120 (Supplemental data 5). Both tested strains had similar optimum growth temperatures (UTEX393: 27.2 °C, SNS0120: 26.8 °C) (Fig. 3 A, B). To compare the overall performance of the two strains, the area under the thermal response curves was calculated, showing that UTEX393 performed almost twice as well (23.9 d^{-1} ·°C) as SNS0120 (12.3 d^{-1}· °C) over the 10 to 40 °C range. Overall, although their thermal optima were very similar, UTEX393 had much stronger growth performance across the full temperature range and was less susceptible to thermal inactivation compared to SNS0120.

3.3. Effect of temperature on photosynthesis

The maximum quantum yield of photosystem II (F_v/F_m) of UTEX393 increased slightly from 0.68 at 10 °C to 0.76 at 28 °C, and a comparable increase was observed for SNS0120 (Fig. 4). At 13 °C and above, the ETR_{max} of UTEX393 was consistently higher than that of SNS0120, and overall both strains showed a decrease in ETR_{max} from 10 °C up to the thermal limit.

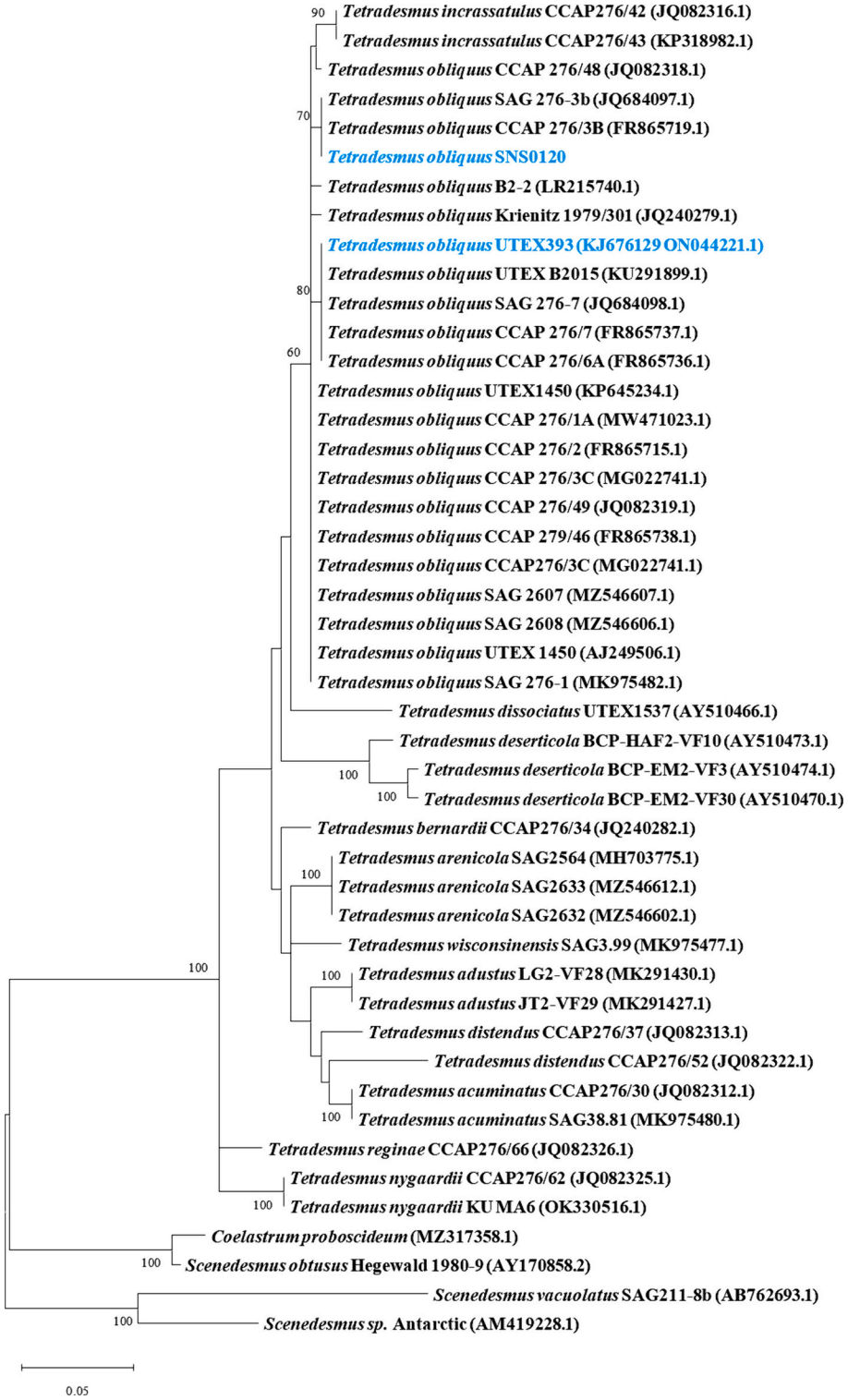

Fig. 2. Maximum likelihood tree of *Tetradesmus obliquus* and other closely related species based on the ITS2 rDNA sequences. The strains used in this study are shown in blue. Numbers next to branches indicate the bootstrap values (1000 replicates). The bootstrap support values above 40 % are shown. *Coelastrum proboscideum* (MZ317358.1), *Scenedesmus obtusus* Hegewald 1980-9 (AY170858.2), *Scenedesmus vacuolatus* SAG 211-8b (AB762693.1), and *Scenedesmus* sp. Antarctica (AM419228.1) serve as the outgroup. (For interpretation of the references to colour in this figure legend, the reader is referred to the web version of this article.)

3.4. Effect of temperature on fatty-acid profiles

The total fatty acid (FA) contents of UTEX393 did not differ significantly from 10 °C to 37 °C (14.5–16.5 % of DW, Table 1). For SNS0120, the total FA contents were lower than UTEX393 measuring 11.0–12.8 % of DW in cultures cultivated at 10 to 31 °C. Fatty acids in both strains were comprised by a large proportion of C18:3*n*-3 and C16:0. Omega-3 polyunsaturated fatty acids (PUFAs) including C16:4*n*-3, C18:3*n*-3, and C18:4*n*-3, showed decreasing trends with increasing temperature, whilst the omega-6 PUFAs including C16:2*n*-6, C18:2*n*-6, and C18:3*n*-6, showed increasing trends as the temperature increased (Fig. 5). The omega-3 to omega-6 ratio decreased from 12.8 ± 0.2 (at 10 °C) to 1.3 ±

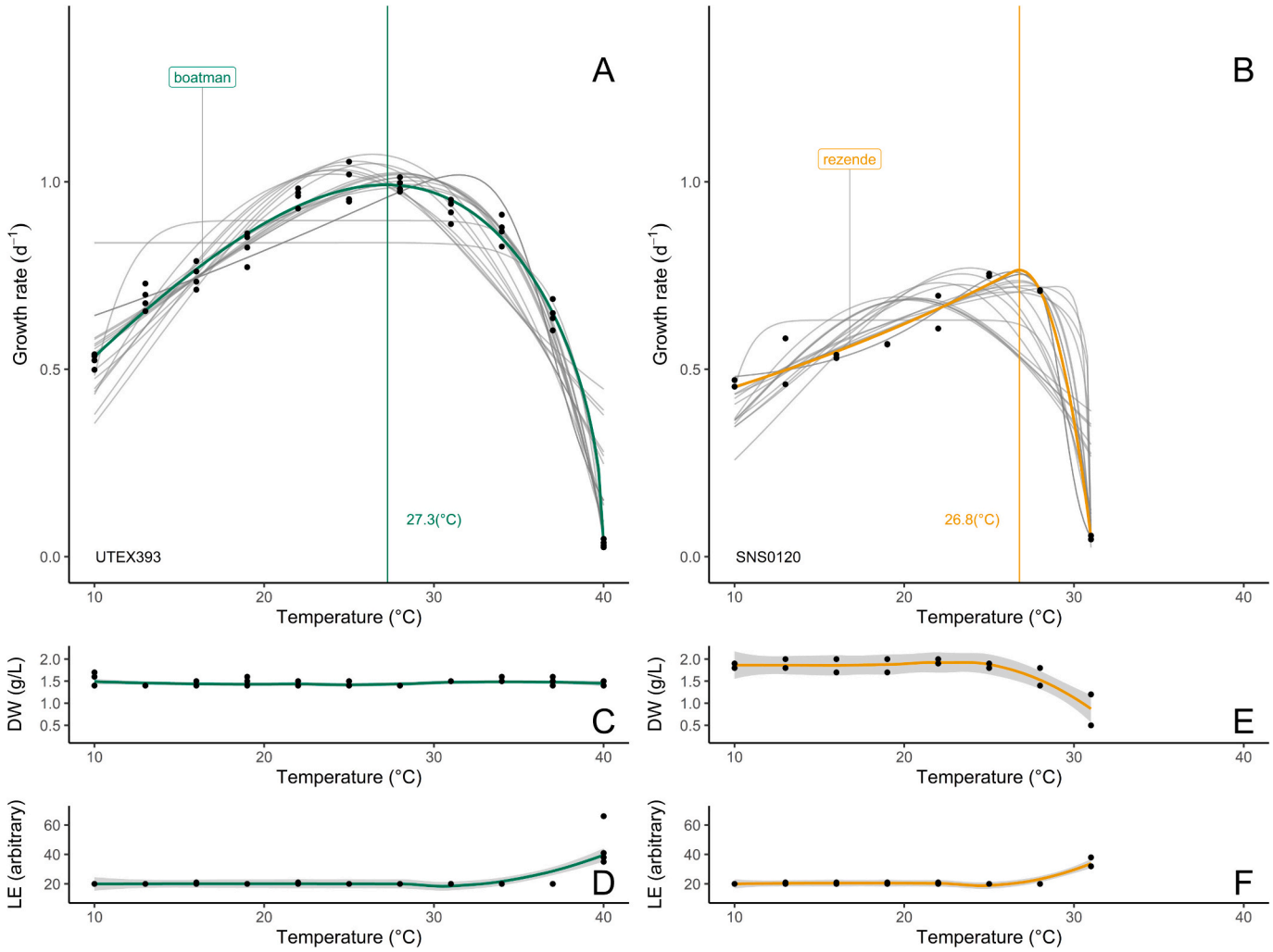

Fig. 3. Growth rates and fitted thermal response models for *Tetradesmus obliquus* UTEX393 (A) and SNS0120 (B). The highlighted lines indicate the best-fitting model for each strain. The biomass concentration in the system (C and E) and transmitted light detected by the secondary light sensor (LE) used for the turbidity control (D and F) are provided. The shaded region represents the confidence intervals (95 % CI). DW: Dry-Weight, LE: Light Emittance.

0.1 (at 40 °C) for UTEX393 and 12.3 ± 0.1 (at 10 °C) to 2.1 ± 0.1 (at 31 °C) for SNS0120 (Fig. 5). Paired *t*-tests between 10 and 25 °C (low-optimum temperature) indicated that the decrease in C18:3*n*-3 and the increase in omega-6 PUFAs (C16:2*n*-6, C18:2*n*-6, and C18:3*n*-6) at optimal temperature were statistically significant ($p < 0.029$). Comparison between 10 and 34 °C (low-high temperature) and between 25 and 34 °C (optimum-high temperature) indicated that the decrease in omega-3 PUFAs (C16:4*n*-3, C18:3*n*-3, and C18:4*n*-3) and the increase in omega-6 PUFAs (C16:2*n*-6, C18:2*n*-6, and C18:3*n*-6) were statistically significant ($p < 0.01$) (Supplemental data 6). For SNS0120, the omega-3 PUFA, C16:4*n*-3 showed a decrease from 8.95 mg/g at 10 °C to 4.16 mg/g at 31 °C. The omega-6 PUFA, C18:3*n*-6 indicated an increase from 0.11 mg/g at 10 °C to 3.37 mg/g at 31 °C (Fig. 5).

3.5. Gene ontology enrichment analysis

Enrichment analysis showed that differentially expressed genes (DEGs) upregulated at 25 °C vs 10 °C were associated with lipid metabolic processes (GO:0006629), transmembrane transport (GO:0055085), negative regulation of transcription by RNA polymerase III (GO:0016480), glycerophospholipid catabolic process (GO:0046475), and phospholipid catabolic process (GO:0009395) (Fig. 6). Downregulated genes at 25 °C vs 10 °C were associated with de novo cotranslational protein folding (GO:0051083), regulation of translational fidelity (GO:0006450), ribosome assembly (GO:0042255), mitochondrial translation (GO:0032543), tetrahydrofolate biosynthetic process (GO:0046654), and response to oxidative stress (GO:0006979) (Fig. 6).

When the temperature was increased from 25 °C to 34 °C, upregulation of the polyamine biosynthetic process (GO:0006596), sucrose metabolic process (GO:0005985), and transmembrane transport (GO:0055085) were detected. Genes associated with photosynthesis and light-harvesting (GO:0009765), proteolysis (GO:0006508), and lipid metabolic process (GO:0006629) were downregulated (Fig. 6).

3.6. Differentially expressed genes (DEG)

Transcriptomic analysis of UTEX393 showed that a total of 4971 genes, 41.5 % of the annotated genes, were significantly differentially expressed ($p < 0.01$) after the temperature was increased from 10 °C (low temperature) to 25 °C (optimal temperature). Log_2 Fold-Changes (Log_2FC) indicated that 2516 of 4971 DEGs were upregulated ($Log_2FC > 0$) while 2455 DEGs were downregulated ($Log_2FC < 0$) (Fig. 7). After increasing the temperature from 25 °C (optimal temperature) to 34 °C (high temperature), a total of 3683 significant DEGs ($p < 0.01$) were identified (30.0 % of total genes). 1915 of 3683 DEGs were upregulated ($Log_2FC > 0$) while 1768 DEGs were downregulated ($Log_2FC < 0$) (Fig. 7).

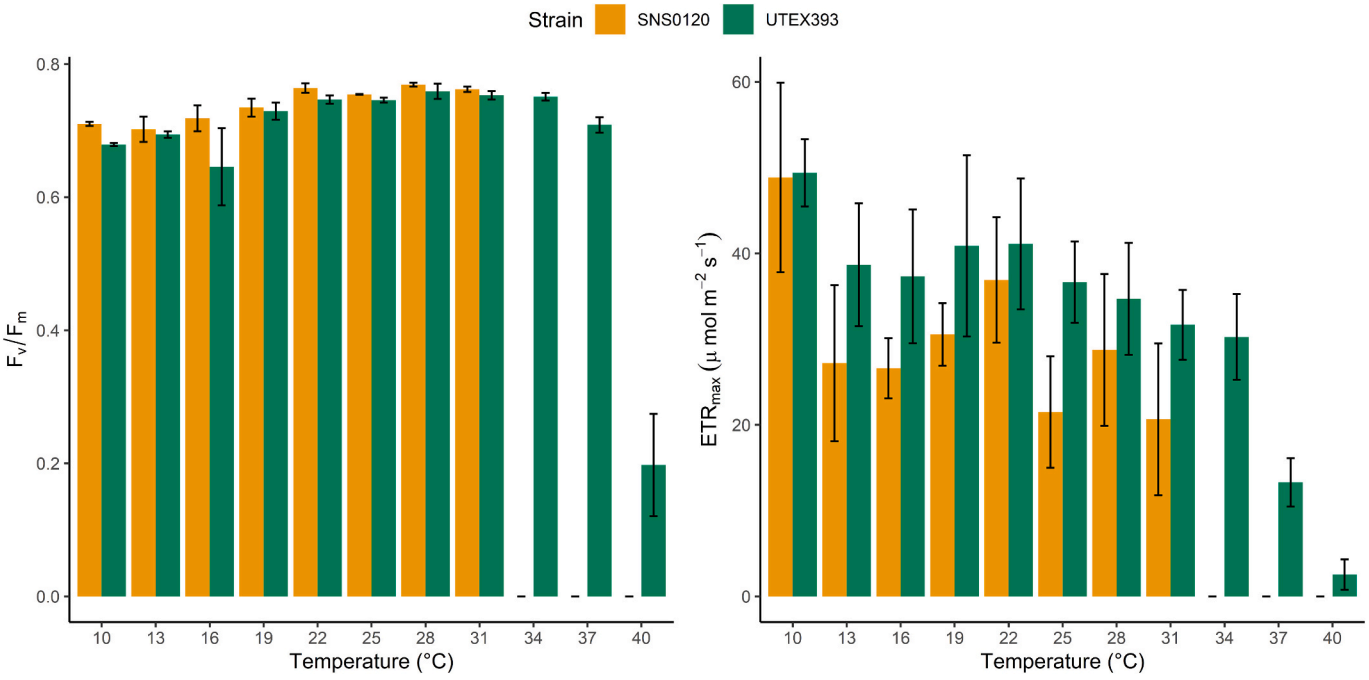

Fig. 4. The F_v/F_m (left) and ETR_{max} (right) at each tested temperature for each strain ($n = 4$ for UTEX393 and $n = 2$ for SNS0120).

Table 1
Total fatty acid contents (% dry mass) of *Tetradesmus obliquus* UTEX393 ($n = 4$) and SNS0120 ($n = 2$) at each tested temperature. Mean ± SD (standard deviation).

Temperature (°C)	10	13	16	19	22	25	28	31	34	37	40
Total fatty acid (%)	Mean ± SD										
UTEX393	15.3 ± 3.1	16.4 ± 0.7	15.3 ± 1	16.4 ± 1.8	17.1 ± 0.6	16.5 ± 1.3	16.9 ± 1.3	16.1 ± 1.5	14.5 ± 0.6	16 ± 1.6	10.6 ± 2.3
SNS0120	12.3 ± 0.5	12.8 ± 0.2	12.1 ± 1.2	14.8 ± 0.4	13.4 ± 0.1	11.6 ± 2.5	12.3 ± 0.6	11 ± 1.8			

The most upregulated DEGs during a temperature upshift from 10 °C to 25 °C included those related to photosynthesis, including chlorophyll *a*-b binding protein (ID:g920.t1, Log_2FC: +6.98, $p = 1.66E-99$), and chlorophyll *a*-b binding protein of LHCII type I (ID:g7543.t1, Log_2FC: +6.17, $p = 6.24E-130$, supplemental data 8). In addition to the top DEGs, upregulation of genes related to lipid metabolism were also detected including digalactosyldiacylglycerol synthase 1 (DGD1, ID: g9689.t1, Log_2FC: +1.15, $p = 8.86E-4$), omega-6 fatty acid desaturase (ID: g1568.t1, Log_2FC: +2.46, $p = 6.67E-78$), omega-3 fatty acid desaturase (ID: g9553.t1, Log_2FC: +0.76, $p = 2.38E-9$), acyl-lipid (7–3)-desaturase (ID: g1477.t1, Log_2FC: +0.47, $p = 3.89E-3$). Genes associated with synthesis or degradation of triacylglycerol (TAG) were moderately upregulated or downregulated from 10 °C to 25 °C, including upregulation of one isoform diacylglycerol *O*-acyltransferase 2 (DGAT2, ID: g15492, Log_2FC: +0.97, $p = 4.3E-3$), and downregulation of two other isoforms of DGAT2, ID: g11201.t1, Log_2FC: −0.67, $p = 8.5E-4$; ID: g5330.t1, Log_2FC: −1.34, $p = 6.65E-7$). The significantly downregulated genes from 10 °C to 25 °C also included 178 ribosomal protein genes, whilst far fewer (35) ribosomal protein genes were significantly upregulated (Supplemental data 8).

From 25 °C to 34 °C, various heat shock proteins including the small heat shock 22 kDa protein (ID: g2965.t1, Log_2FC: +4.04, $p = 1.01E-19$, ID: g9776.t1, Log_2FC: +1.70, $p = 2.68E-4$) and heat shock protein HSP 90-beta (ID: g14235.t1, Log_2FC: +0.97, $p = 6.38E-07$), and the activator of 90 kDa heat shock protein ATPase homolog 2 (ID: g13263.t1, Log_2FC: +0.65, $p = 1.42E-3$), as well as other genes associated with stress response including auxin transporter protein 1 (ID: g8745.t1, Log_2FC: +0.84, $p = 6.41E-3$), indole-3-glycerol phosphate synthase (ID: g8367.t1, Log_2FC: +0.59, $p = 1.12E-3$), and ornithine decarboxylase (ODC1, ID: g6244.t1, Log_2FC: +3.15, $p = 5.09E-29$) were significantly upregulated. Expression of a number of fatty acid desaturase genes was downregulated from 25 °C to 34 °C, including stearoyl-[acyl-carrier-protein] 9-desaturase (ID: g13937.t1, Log_2FC: −0.94, $p = 1.03$ E-4), omega-3 fatty acid desaturases (ID: g11877.t1, Log_2FC: −0.62, $p = 1.08E-4$; ID: g7406.t1, Log_2FC: −1.97, $p = 1.39E-36$), omega-6 fatty acid desaturase (ID:g2919.t1, Log_2FC: −0.98, $p = 7.17E-6$), acyl-lipid (7–3)-desaturase (ID: g13617.t1, Log_2FC: −1.16, $p = 8.53E-5$; ID: g899.t1, Log_2FC:-1.14, $p = 6.3E-7$), delta (12) fatty acid desaturase (ID: g6149.t1, Log_2FC:-1.03, $p = 2.74E-8$), acyl-CoA desaturase (ID:g1292.t1, Log_2FC:-1.01, $p = 2.19E-3$; ID:g2041.t1, Log_2FC: −0.69, $p = 3.23E-4$) and no fatty acid desaturases were upregulated. Many genes associated with de novo fatty acid synthesis were also downregulated from 25 °C to 34 °C, including 3-oxoacyl-acyl-carrier-protein (ACP) synthase 2 (ID: g9377.t1, Log_2FC:-1.09, $p = 4.33E-17$; ID: g11737.t1, Log_2FC: −1.00, $p = 1.9E-4$), 3-oxoacyl-[acyl-carrier-protein] reductase (ID:g12323.t1, Log_2FC:-1.15, $p = 3.49E-3$), 3-ketoacyl-CoA synthase 9 (ID:g16260.t1, Log_2FC:-0.87, $p = 6.49E-5$), malonyl CoA-acyl carrier protein transacylase (ID:g15800.t1, Log_2FC:-1.58, $p = 2.66E-30$), acyl carrier protein (ID: g12952.t1, Log_2FC: −0.66, $p = 4.24E-4$), acetyl-coenzyme A carboxylase carboxyl transferase subunit alpha (ID: g5710.t1, Log_2FC: −0.46, $p = 2.66E-3$), biotin carboxyl carrier protein of acetyl-CoA carboxylase (ID:g8208.t1, Log_2FC:-0.81, $p = 9.55E-6$), and enoyl-[acyl-carrier-protein] reductase (ID: g14618.t1, Log_2FC: −0.67, $p = 6.17E-7$). DGD1, the gene strongly upregulated from 10 °C to 25 °C, was slightly downregulated (ID: g9655.t1, Log_2FC: −0.61, $p = 1.08E-4$) from 25 °C to 34 °C.

4. Discussion

The results show that the two strains of *Tetradesmus obliquus* had profoundly different thermal tolerance profiles. This was surprising

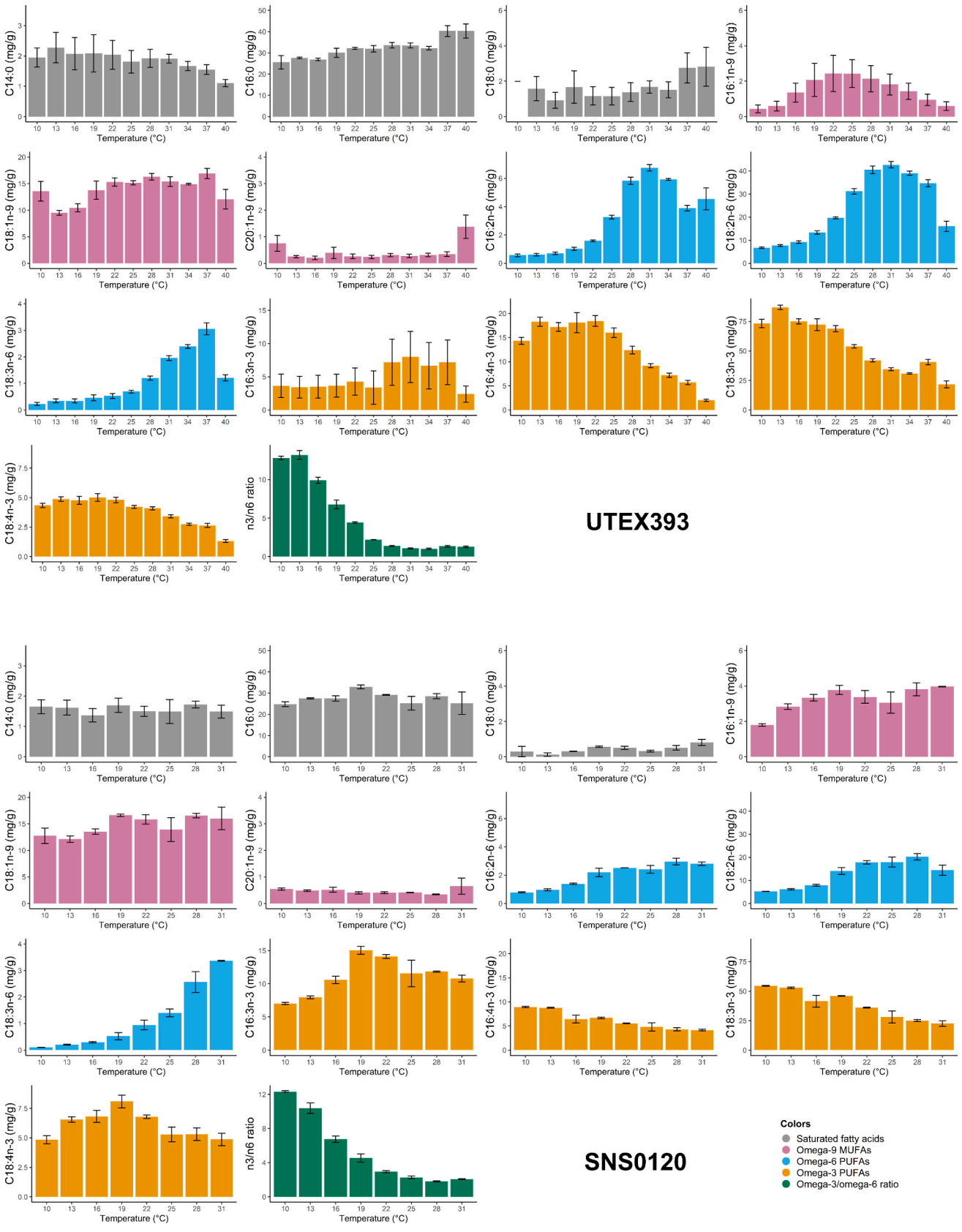

Fig. 5. Contents of each fatty acid (mg/g DW) in UTEX 393 at temperatures between 10 °C to 40 °C ($n = 4$) and in the SNS0120 at temperatures between 10 °C to 31 °C ($n = 2$).

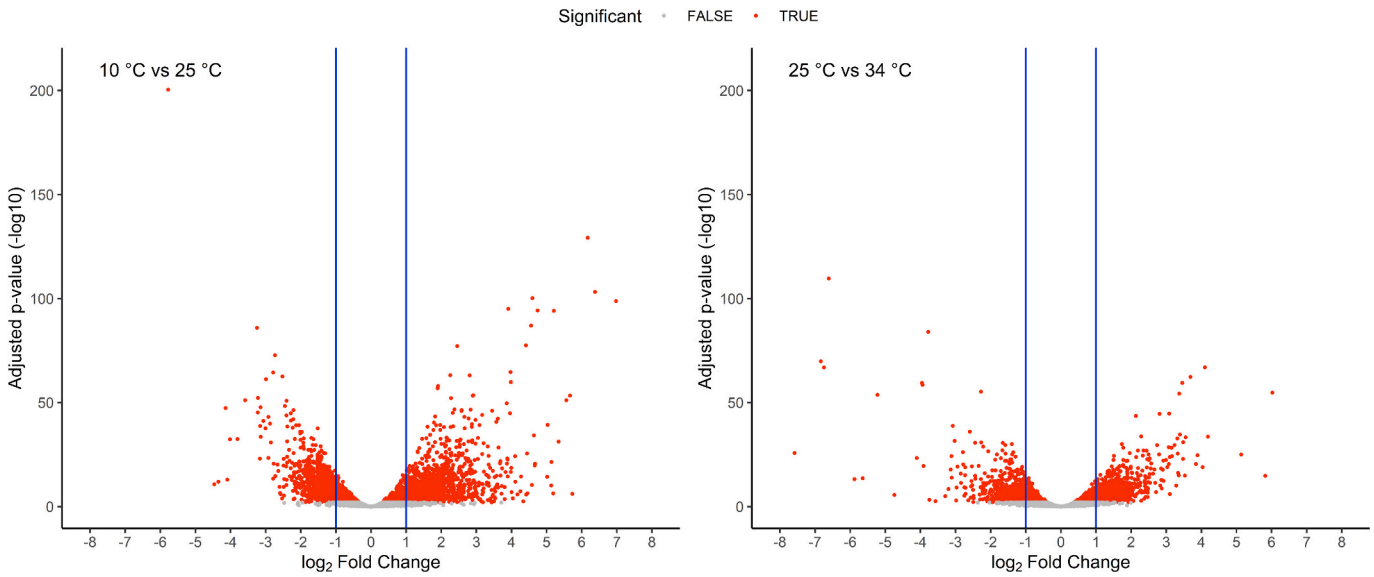

Fig. 6. Summary of the biological process GO terms at 10 °C vs 25 °C and 25 °C vs 34 °C which showed statistical significance ($p < 0.05$, $n = 4$). -Log10 p-value: -log10 of adjusted p-values calculated by using the Benjamini-Hochberg method. A more detailed summary of the significant biological processes, molecular functions, and cell component GO terms and related genes are shown in Supplemental data 7.

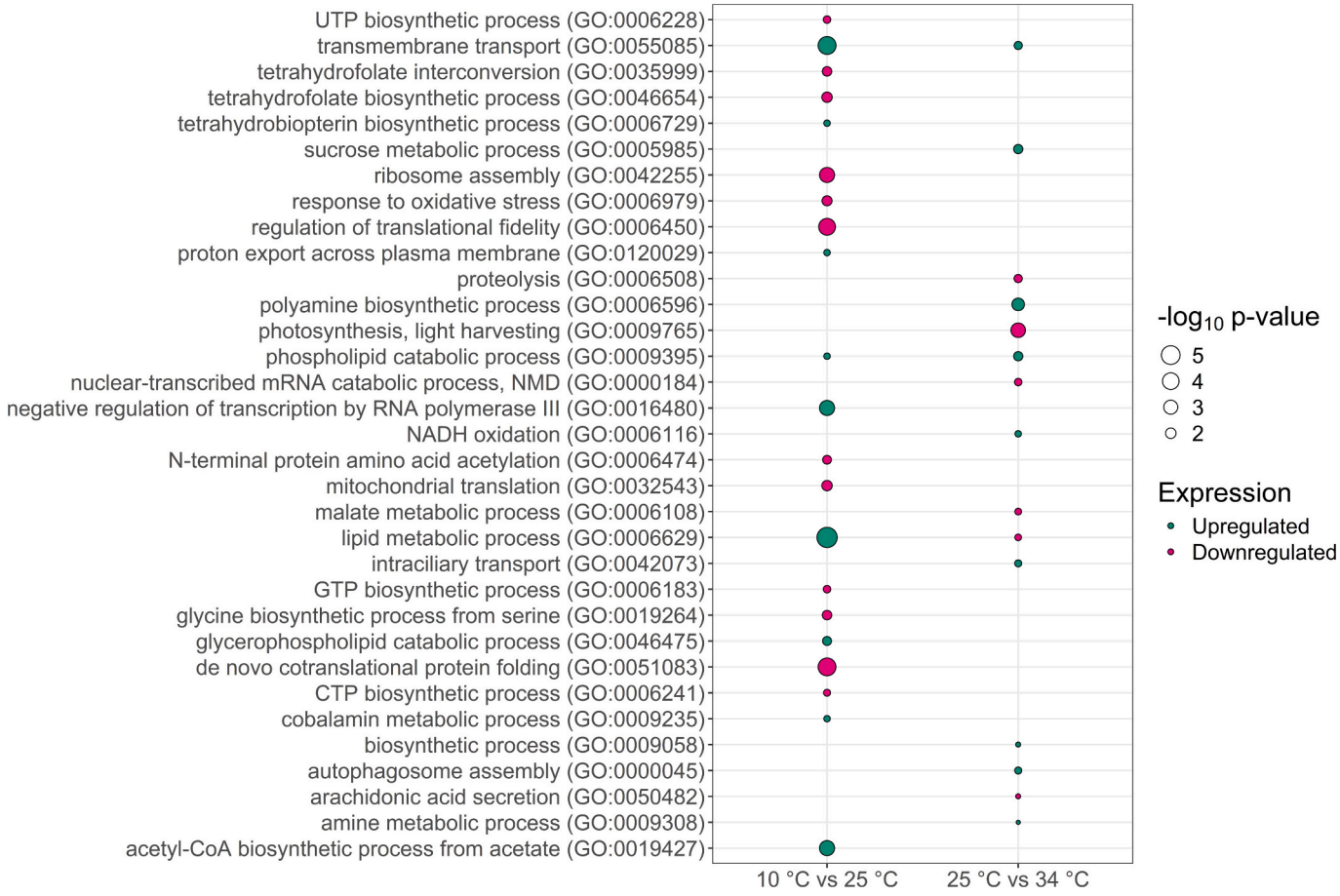

Fig. 7. Significantly differentially expressed genes in strain UTEX393 after the temperature was increased from 10 °C to 25 °C (left) as well as from 25 °C to 34 °C (right). Blue vertical lines: indicate the $\log_2$FC values at −1 and 1 ($n = 4$). (For interpretation of the references to colour in this figure legend, the reader is referred to the web version of this article.)

considering the phylogenetic proximity of both strains, which differed by only 2 bp in the alignment of the hypervariable ITS2 rDNA sequences. Strain UTEX393 exhibited a wider thermal tolerance range and exhibited substantially better growth performance than SNS0120, making it more practical to cultivate throughout the year in outdoor cultivation systems that can experience major shifts in temperature both daily and seasonally. In comparison, strain SNS0120 may require more careful monitoring and control of the cultivation temperature. Understanding the overall differences in thermal response between strains will help maximize the efficiency of biomass production, avoid failure of cultivations, and thereby reduce operating costs in large-scale cultivation.

Using turbidity control and supply of excess nutrients, we showed that temperature did not affect the amount of total fatty acids in *T. obliquus*. However, temperature remodelled the fatty acid profiles of both strains, where the ratio of omega-3 to omega-6 fatty acids decreased toward higher temperatures. Similar behaviour of the C18 omega-3 and omega-6 PUFAs has been observed in several other microalgae species (Aussant et al., 2018; Degraeve-Guilbault et al., 2021; Fuschino et al., 2011). The data indicate that in large-scale cultivations, shifts in cultivation temperature in the order of 5 to 20 °C, perhaps occurring seasonally, may drive moderate but detectable changes in the fatty acid profile that ultimately impact the biomass product quality. Under the nutrient-sufficient conditions applied in our experiments, the majority of fatty acids are incorporated in polar membrane lipids (e.g. DGDG and MGDG, gene expressions will be discussed later) that have structural and functional roles in different subcellular components in response to the ambient temperature (Calhoun et al., 2021; Li-Beisson et al., 2015; Suzuki et al., 2023). The remodeling of the fatty-acid profile with temperature thus implies the adjustment of membrane lipid properties, and/or changes in the size or proportion of cell internal organelles and compartments (Barten et al., 2021).

The turbidostat cultivations also generated temperature-induced variation in the growth rate, which approximately doubled from 0.52 d^{-1} at 10 °C to 0.99 d^{-1} at 25 °C in UTEX393. The growth rate hypothesis describes an expected correlation between the cell growth rate, ribosome abundance, and cellular elemental stoichiometry (Rees and Raven, 2021). We therefore anticipated that patterns in gene expression from low (10 °C) to optimal (25 °C) temperature might reflect altered metabolic pathways associated with the change in growth rate, particularly genes associated with translation, ribosome biosynthesis, and protein turnover. Though, some genes associated with the GO terms ribosomal biogenesis (GO:0042254) and translation (GO:0006412) were significantly upregulated at 25 °C vs 10 °C, our results indicated that a substantially larger number of ribosomal genes were significantly downregulated (Supplemental data 8). This result was unexpected, but it suggests that cellular translation machinery is not a bottleneck for supporting accelerated growth rate due to the effect of higher temperature alone. On the contrary, alternative strategies used by microbes for allocating resources may support higher growth rates in response to changes in the environment (Basan et al., 2020; Hidalgo et al., 2022; León-Vaz et al., 2023). Our data invites further studies for both industry and climate-driven effects of temperature on microalgae growth in nature. Especially, the effects of dynamic temperature change experienced in outdoor cultivation systems, and the effects of adaptation to different thermal regimes, should be investigated.

Transcriptomic analysis of differentially expressed genes in strain UTEX393 provides comprehensive insight into the extensive molecular regulation and metabolic pathway remodeling that underpins short-term acclimation from low to optimal temperature (10 to 25 °C), and from optimal to elevated thermal stress (25 to 34 °C). A large number of genes, representing 30 and 41.5 % of the annotated strain UTEX393 protein coding sequences, were significantly differentially expressed in each of the respective temperature comparisons. Enrichment analysis of the gene ontology (GO) terms showed that lipid metabolic processes (GO:0006629) were the most affected biological pathways by a temperature increase from low temperature (10 °C) to optimal temperature (25 °C), highlighting the importance of lipid metabolism as a major thermal acclimation strategy. We observed significant upregulation of gene digalactosyldiacylglycerol synthase (Log_2FC: +1.15), which catalyses the formation of DGDG from MGDG as part of membrane response from low to optimum temperature. The ratio of bilayer forming lipids (i.e., DGDG) to non-bilayer forming lipids (i.e., MGDG) have been shown to increase as temperature rises to maintain membrane fluidity in higher plants and algae (Légeret et al., 2016; Zheng et al., 2011). On the contrary, DGD1 was slightly downregulated (Log_2FC: −0.61) under thermal stress at 34 °C, and may be associated with downregulation of photosynthesis and light harvesting processes (GO:0009765), because DGDG synthesis is tightly regulated with the formation of the photosynthetic chlorophyll-protein complexes in the thylakoid membrane (Kobayashi et al., 2014).

A notable change was observed in the expression of fatty-acid desaturase genes, which regulate the FA profiles. The omega-6 fatty acid desaturase Δ12 FAD converts C16:1n-9 or C18:1n-9 to C16:2n-6 or C18:2n-6 by inserting a double bond at the omega-6 position, while omega-3 fatty acid desaturases introduce a double bond at the omega-3 position, leading to conversion of omega-6 fatty acids including C16:2n-6, C16:3n-6, C18:2n-6, C18:3n-6 into omega-3 fatty acids (Guschina and Harwood, 2006; Zhou et al., 2023). Upregulation of omega-3 fatty acid desaturase expression has been observed in *Chlorella vulgaris* and *Chlamydomonas reinhardtii* under cold-stress (Nguyen et al., 2013; Suga et al., 2002), while heat stress caused downregulation of omega-6 fatty acid desaturase expression in *C. reinhardtii* (Légeret et al., 2016). In our study, from low (10 °C) to optimal (25 °C) temperature, a chloroplastic omega-6 fatty acid desaturase was significantly upregulated (Log_2FC: +2.46), a second isoform was downregulated to a lesser extent (Log_2FC: −0.98), while two chloroplastic omega-3 fatty acid desaturases were downregulated (Log_2FC: −0.62 and -1.97). Overall, the altered expression of these four desaturases were broadly consistent with phenotypic changes in the increase of C16:2n-6 and C18:2n-6, as well as an overall decrease in the omega-3/omega-6 FA ratio (Fig. 5). The same omega-3 fatty acid desaturases were further downregulated (Log_2FC: −1.00 and -0.57, respectively) from optimal temperature to thermal stress (25 to 34 °C), which was associated with the lower omega-3/omega-6 FA ratios observed at 34 °C. Lastly, we show that from optimal to higher temperatures (25 to 34 °C), the expression of two acyl-lipid (7–3) desaturases (Delta-4 desaturase) were significantly downregulated (Log_2FC: −2.31 and -2.18). The desaturase is known to convert 16:3n-3 into C16:4n-3, and the amount of C16:4n-3 was also inversely related with temperature from 25 °C to 34 °C. The decrease of C16:4n-3 with increased temperature has been previously reported in *T. obliquus* (Fuschino et al., 2011), and other green algae including *Chlamydomonas malina* (Morales-Sánchez et al., 2020). As C16:4n-3 is mainly located in MGDG in Fuschino et al. (2011), and known to be exclusively synthesized in the chloroplast of *C. reinhardtii* (Giroud et al., 1988), the observed downregulation of these genes and reduced amount of C16:4n-3 at high temperature may be connected to the downregulation of photosynthesis and light harvesting processes (GO:0009765).

5. Conclusion

Examining the thermal performance of algal strains is important for the selection of robust algae for year-round cultivation at a given location, thereby maximizing yields and biomass quality while reducing operating costs. Our study highlighted the contrasting growth profiles of two *Tetradesmus* strains cultivated across a large thermal range, and also showed that temperature alters the composition of industrially valuable components including omega-3 and omega-6 fatty acids. Transcriptomic analysis of strain UTEX393 captured the cell-wide metabolic adjustments from low to optimal, and optimal to high temperature, providing evidence for the roles of lipid metabolism and ribosome activity that take place under temperature change. Thermal screening has the potential to substantially improve yields and choose amongst microalgal

strains for maximizing production in different climates.

Supplementary data to this article can be found online at https://doi.org/10.1016/j.biteb.2024.101909.

CRediT authorship contribution statement

Hidehiko Kato: Writing – original draft, Formal analysis, Data curation, Conceptualization, Investigation, Methodology, Validation, Visualization, Writing – review & editing. **Hirono Suzuki:** Data curation, Conceptualization, Formal analysis, Investigation, Methodology, Supervision, Validation, Visualization, Writing – review & editing. **René H. Wijffels:** Resources. **Peter S.C. Schulze:** Resources, Conceptualization. **Chris J. Hulatt:** Supervision, Conceptualization, Formal analysis, Investigation, Methodology, Resources, Validation, Writing – review & editing.

Declaration of competing interest

The authors declare that they have no known competing financial interests or personal relationships that could have appeared to influence the work reported in this paper.

Data availability

Data will be made available on request.

Acknowledgement

The present work was part of the AlgaCycle project, designated as PT-INNOVATION-0023, funded by Iceland, Liechtenstein and Norway through the EEA and Norway Grants within the scope of the Blue Growth Program. We also thank Anjana Palihawadana for his support in fatty acids analysis.

References

Alexa, A., Rahnenfuhrer, J., 2021. topGO: enrichment analysis for gene ontology. In: R Package Version 2.46.0. https://doi.org/10.18129/B9.bioc.topGO.

Angilletta, M.J., 2006. Estimating and comparing thermal performance curves. J. Therm. Biol. 31, 541–545. https://doi.org/10.1016/j.jtherbio.2006.06.002.

Aussant, J., Guihéneuf, F., Stengel, D.B., 2018. Impact of temperature on fatty acid composition and nutritional value in eight species of microalgae. Appl. Microbiol. Biotechnol. 102, 5279–5297. https://doi.org/10.1007/s00253-018-9001-x.

Barten, R., Djohan, Y., Evers, W., Wijffels, R., Barbosa, M., 2021. Towards industrial production of microalgae without temperature control: the effect of diel temperature fluctuations on microalgal physiology. J. Biotechnol. 336, 56–63. https://doi.org/10.1016/j.jbiotec.2021.06.017.

Basan, M., Honda, T., Christodoulou, D., Hörl, M., Chang, Y.-F., Leoncini, E., Mukherjee, A., Okano, H., Taylor, B.R., Silverman, J.M., Sanchez, C., Williamson, J. R., Paulsson, J., Hwa, T., Sauer, U., 2020. A universal trade-off between growth and lag in fluctuating environments. Nature 584, 470–474. https://doi.org/10.1038/s41586-020-2505-4.

Béchet, Q., Muñoz, R., Shilton, A., Guieysse, B., 2013. Outdoor cultivation of temperature-tolerant *Chlorella sorokiniana* in a column photobioreactor under low power-input. Biotechnol. Bioeng. 110, 118–126. https://doi.org/10.1002/bit.24603.

Bischoff, H.W., Bold, H.C., 1963. Phycological Studies IV. Some Soil Algae From Enchanted Rock and Related Algal Species.

Bleeke, F., Rwehumbiza, V.M., Winckelmann, D., Klöck, G., 2014. Isolation and characterization of new temperature tolerant microalgal strains for biomass production. Energies 7, 7847–7856. https://doi.org/10.3390/en7127847.

Boatman, T.G., Lawson, T., Geider, R.J., 2017. A key marine diazotroph in a changing ocean: the interacting effects of temperature, CO2 and light on the growth of *Trichodesmium erythraeum* IMS101. PLoS One 12, e0168796. https://doi.org/10.1371/journal.pone.0168796.

Breuer, G., Lamers, P.P., Martens, D.E., Draaisma, R.B., Wijffels, R.H., 2012. The impact of nitrogen starvation on the dynamics of triacylglycerol accumulation in nine microalgae strains. Bioresour. Technol. 124, 217–226. https://doi.org/10.1016/j.biortech.2012.08.003.

Briere, J.-F., Pracros, P., Le Roux, A.-Y., Pierre, J.-S., 1999. A novel rate model of temperature-dependent development for arthropods. Environ. Entomol. 28, 22–29. https://doi.org/10.1093/ee/28.1.22.

Calhoun, S., Bell, T.A.S., Dahlin, L.R., Kunde, Y., LaButti, K., Louie, K.B., Kuftin, A., Treen, D., Dilworth, D., Mihaltcheva, S., Daum, C., Bowen, B.P., Northen, T.R., Guarnieri, M.T., Starkenburg, S.R., Grigoriev, I.V., 2021. A multi-omic characterization of temperature stress in a halotolerant *Scenedesmus* strain for algal biotechnology. Commun. Biol. 4, 1–15. https://doi.org/10.1038/s42003-021-01859-y.

Casagli, F., Bernard, O., 2022. How heat transfer indirectly affects performance of algae-bacteria raceways. Microorganisms 10, 1515. https://doi.org/10.3390/microorganisms10081515.

Cheregi, O., Engelbrektsson, J., Andersson, M.X., Strömberg, N., Ekendahl, S., Godhe, A., Spetea, C., 2021. Marine microalgae for outdoor biomass production—a laboratory study simulating seasonal light and temperature for the west coast of Sweden. Physiol. Plant. 173, 543–554. https://doi.org/10.1111/ppl.13412.

Degraeve-Guilbault, C., Pankasem, N., Gueirrero, M., Lemoigne, C., Domergue, F., Kotajima, T., Suzuki, I., Joubès, J., Corellou, F., 2021. Temperature acclimation of the picoalga *Ostreococcus tauri* triggers early fatty-acid variations and involves a plastidial ω3-desaturase. Front. Plant Sci. 12, 639330 https://doi.org/10.3389/fpls.2021.639330.

DeLong, J.P., Gibert, J.P., Luhring, T.M., Bachman, G., Reed, B., Neyer, A., Montooth, K. L., 2017. The combined effects of reactant kinetics and enzyme stability explain the temperature dependence of metabolic rates. Ecol. Evol. 7, 3940–3950. https://doi.org/10.1002/ece3.2955.

Erbland, P., Caron, S., Peterson, M., Alyokhin, A., 2020. Design and performance of a low-cost, automated, large-scale photobioreactor for microalgae production. Aquac. Eng. 90, 102103 https://doi.org/10.1016/j.aquaeng.2020.102103.

Flinn, P.W., 1991. Temperature-dependent functional response of the parasitoid *Cephalonomia waterstoni* (Gahan) (Hymenoptera: *Bethylidae*) attacking rusty grain beetle larvae (Coleoptera: *Cucujidae*). Environ. Entomol. 20, 872–876. https://doi.org/10.1093/ee/20.3.872.

Flynn, K.J., Raven, J.A., Rees, T.A.V., Finkel, Z., Quigg, A., Beardall, J., 2010. Is the growth rate hypothesis applicable to microalgae? J. Phycol. 46, 1–12. https://doi.org/10.1111/j.1529-8817.2009.00756.x.

Fuschino, J.R., Guschina, I.A., Dobson, G., Yan, N.D., Harwood, J.L., Arts, M.T., 2011. Rising water temperatures alter lipid dynamics and reduce N-3 essential fatty acid concentrations in *Scenedesmus Obliquus* (chlorophyta). J. Phycol. 47, 763–774. https://doi.org/10.1111/j.1529-8817.2011.01024.x.

Gabriel, H., 2020. Theory and Practice of Random Effects and REML in variancePartition and Dream.

Genty, B., Briantais, J.-M., Baker, N.R., 1989. The relationship between the quantum yield of photosynthetic electron transport and quenching of chlorophyll fluorescence. Biochim. Biophys. Acta Gen. Subj. 990, 87–92. https://doi.org/10.1016/S0304-4165(89)80016-9.

Gifuni, I., Pollio, A., Safi, C., Marzocchella, A., Olivieri, G., 2019. Current bottlenecks and challenges of the microalgal biorefinery. Trends Biotechnol. 37, 242–252. https://doi.org/10.1016/j.tibtech.2018.09.006.

Giroud, C., Gerber, A., Eichenberger, W., 1988. Lipids of *Chlamydomonas reinhardtii*. Analysis of molecular species and intracellular site(s) of biosynthesis. Plant Cell Physiol. 29, 587–595. https://doi.org/10.1093/oxfordjournals.pcp.a077533.

Guschina, I.A., Harwood, J.L., 2006. Lipids and lipid metabolism in eukaryotic algae. Prog. Lipid Res. 45, 160–186. https://doi.org/10.1016/j.plipres.2006.01.001.

Handler, R.M., Shonnard, D.R., Kalnes, T.N., Lupton, F.S., 2014. Life cycle assessment of algal biofuels: influence of feedstock cultivation systems and conversion platforms. Algal Res. 4, 105–115. https://doi.org/10.1016/j.algal.2013.12.001.

Hidalgo, D., Martínez-Ortiz, C.A., Palsson, B.O., Jiménez, J.I., Utrilla, J., 2022. Regulatory perturbations of ribosome allocation in bacteria reshape the growth proteome with a trade-off in adaptation capacity. iScience 25, 103879. https://doi.org/10.1016/j.isci.2022.103879.

Hinshelwood, C.N., 1946. The chemical kinetics of the bacterial cell. Oxford University Press.

Hoff, K.J., Lange, S., Lomsadze, A., Borodovsky, M., Stanke, M., 2016. BRAKER1: unsupervised RNA-Seq-based genome annotation with GeneMark-ET and AUGUSTUS. Bioinformatics 32, 767–769. https://doi.org/10.1093/bioinformatics/btv661.

Hoffman, G.E., Roussos, P., 2021. Dream: powerful differential expression analysis for repeated measures designs. Bioinformatics 37, 192–201. https://doi.org/10.1093/bioinformatics/btaa687.

Hoffman, G.E., Schadt, E.E., 2016. variancePartition: interpreting drivers of variation in complex gene expression studies. BMC Bioinform. 17, 483. https://doi.org/10.1186/s12859-016-1323-z.

Huang, Q., Jiang, F., Wang, L., Yang, C., 2017. Design of photobioreactors for mass cultivation of photosynthetic organisms. Engineering 3, 318–329. https://doi.org/10.1016/J.ENG.2017.03.020.

Huertas, I.E., Rouco, M., López-Rodas, V., Costas, E., 2011. Warming will affect phytoplankton differently: evidence through a mechanistic approach. Proc. R. Soc. B Biol. Sci. 278, 3534–3543. https://doi.org/10.1098/rspb.2011.0160.

Huesemann, M., Edmundson, S., Gao, S., Negi, S., Dale, T., Gutknecht, A., Daligault, H.E., Carr, C.K., Freeman, J., Kern, T., Starkenburg, S.R., Gleasner, C.D., Louie, W., Kruk, R., McGuire, S., 2023. DISCOVR strain pipeline screening – part I: maximum specific growth rate as a function of temperature and salinity for 38 candidate microalgae for biofuels production. Algal Res. 71, 102996 https://doi.org/10.1016/j.algal.2023.102996.

Huete-Stauffer, T.M., Arandia-Gorostidi, N., Díaz-Pérez, L., Morán, X.A.G., 2015. Temperature dependences of growth rates and carrying capacities of marine bacteria depart from metabolic theoretical predictions. FEMS Microbiol. Ecol. 91, fiv111. https://doi.org/10.1093/femsec/fiv111.

Hulatt, C.J., Smolina, I., Dowle, A., Kopp, M., Vasanth, G.K., Hoarau, G.G., Wijffels, R.H., Kiron, V., 2020. Proteomic and transcriptomic patterns during lipid remodeling in *Nannochloropsis gaditana*. Int. J. Mol. Sci. 21, 6946. https://doi.org/10.3390/ijms21186946.

Hulatt, C.J., Wijffels, R.H., Posewitz, M.C., 2021. The Genome of the haptophyte *Diacronema lutheri* (*Pavlova lutheri*, Pavlovales): a model for lipid biosynthesis in eukaryotic algae. Genome Biol. Evol. 13, evab178. https://doi.org/10.1093/gbe/evab178.

Jöhnk, K.D., Huisman, J., Sharples, J., Sommeijer, B., Visser, P.M., Stroom, J.M., 2008. Summer heatwaves promote blooms of harmful cyanobacteria. Glob. Chang. Biol. 14, 495–512. https://doi.org/10.1111/j.1365-2486.2007.01510.x.

Johnson, F.H., Lewin, I., 1946. The growth rate of E. coli in relation to temperature, quinine and coenzyme. J. Cell. Comp. Physiol. 28, 47–75. https://doi.org/10.1002/jcp.1030280104.

Kamykowski, D., 1985. A survey of protozoan laboratory temperature studies applied to marine dinoflagellate behavior from a field perspective. Contrib. Mar. Sci. 1985.

Kitajima, M., Butler, W.L., 1975. Quenching of chlorophyll fluorescence and primary photochemistry in chloroplasts by dibromothymoquinone. Biochim. Biophys. Acta 376, 105–115. https://doi.org/10.1016/0005-2728(75)90209-1.

van der Knaap, J.A., Verrijzer, C.P., 2016. Undercover: gene control by metabolites and metabolic enzymes. Genes Dev. 30, 2345–2369. https://doi.org/10.1101/gad.289140.116.

Kobayashi, K., Fujii, S., Sasaki, D., Baba, S., Ohta, H., Masuda, T., Wada, H., 2014. Transcriptional regulation of thylakoid galactolipid biosynthesis coordinated with chlorophyll biosynthesis during the development of chloroplasts in Arabidopsis. Front. Plant Sci. 5 https://doi.org/10.3389/fpls.2014.00272.

Kontopoulos, D.-G., García-Carreras, B., Sal, S., Smith, T.P., Pawar, S., 2018. Use and misuse of temperature normalisation in meta-analyses of thermal responses of biological traits. PeerJ 6, e4363. https://doi.org/10.7717/peerj.4363.

Kumar, S., Stecher, G., Li, M., Knyaz, C., Tamura, K., 2018. MEGA X: Molecular evolutionary genetics analysis across computing platforms. Mol. Biol. Evol. 35, 1547–1549. https://doi.org/10.1093/molbev/msy096.

Lactin, D.J., Holliday, N.J., Johnson, D.L., Craigen, R., 1995. Improved rate model of temperature-dependent development by arthropods. Environ. Entomol. 24, 68–75.

Lage, S., Toffolo, A., Gentili, F.G., 2021. Microalgal growth, nitrogen uptake and storage, and dissolved oxygen production in a polyculture based-open pond fed with municipal wastewater in northern Sweden. Chemosphere 276, 130122. https://doi.org/10.1016/j.chemosphere.2021.130122.

Law, C.W., Chen, Y., Shi, W., Smyth, G.K., 2014. voom: precision weights unlock linear model analysis tools for RNA-seq read counts. Genome Biol. 15, R29. https://doi.org/10.1186/gb-2014-15-2-r29.

Légeret, B., Schulz-Raffelt, M., Nguyen, H.M., Auroy, P., Beisson, F., Peltier, G., Blanc, G., Li-Beisson, Y., 2016. Lipidomic and transcriptomic analyses of *Chlamydomonas reinhardtii* under heat stress unveil a direct route for the conversion of membrane lipids into storage lipids. Plant Cell Environ. 39, 834–847. https://doi.org/10.1111/pce.12656.

León-Vaz, A., León, R., Vigara, J., Funk, C., 2023. Exploring Nordic microalgae as a potential novel source of antioxidant and bioactive compounds. New Biotechnol. 73, 1–8. https://doi.org/10.1016/j.nbt.2022.12.001.

Liao, Y., Smyth, G.K., Shi, W., 2014. featureCounts: an efficient general purpose program for assigning sequence reads to genomic features. Bioinformatics 30, 923–930. https://doi.org/10.1093/bioinformatics/btt656.

Li-Beisson, Y., Beisson, F., Riekhof, W., 2015. Metabolism of acyl-lipids in *Chlamydomonas reinhardtii*. Plant J. 82 (3), 504–522. https://doi.org/10.1111/tpj.12787.

Lin, Z., Zhou, J., He, L., He, X., Pan, Z., Wang, Y., He, Q., 2022. High-temperature biofilm system based on heterotrophic nitrification and aerobic denitrification treating high-strength ammonia wastewater: Nitrogen removal performances and temperature-regulated metabolic pathways. Bioresour. Technol. 344, 126184 https://doi.org/10.1016/j.biortech.2021.126184.

Lynch, M., Gabriel, W., 1987. Environmental tolerance. Am. Nat. 129, 283–303. https://doi.org/10.1086/284635.

Millington, R., Cox, P., Moore, J., Yvon-Durocher, G., 2019. Modelling ecosystem adaptation and dangerous rates of global warming. Emerg. Top. Life Sci. 3, ETLS20180113 https://doi.org/10.1042/ETLS20180113.

Milward, E.A., Shahandeh, A., Heidari, M., Johnstone, D.M., Daneshi, N., Hondermarck, H., 2016. Transcriptomics. In: Bradshaw, R.A., Stahl, P.D., Bradshaw, R.A., Stahl, P.D. (Eds.), Encyclopedia of Cell Biology. Waltham, pp. 160–165.

Montagnes, D.J.S., Morgan, G., Bissinger, J.E., Atkinson, D., Weisse, T., 2008. Short-term temperature change may impact freshwater carbon flux: a microbial perspective. Glob. Chang. Biol. 14, 2823–2838. https://doi.org/10.1111/j.1365-2486.2008.01700.x.

Morales-Sánchez, D., Schulze, P.S.C., Kiron, V., Wijffels, R.H., 2020. Temperature-dependent lipid accumulation in the polar marine microalga *Chlamydomonas malina* RCC2488. Front. Plant Sci. 11.

Nguyen, H.M., Cuiné, S., Beyly-Adriano, A., Légeret, B., Billon, E., Auroy, P., Beisson, F., Peltier, G., Li-Beisson, Y., 2013. The green microalga *Chlamydomonas reinhardtii* has a single ω-3 fatty acid desaturase that localizes to the chloroplast and impacts both plastidic and extraplastidic membrane lipids. Plant Physiol. 163, 914–928. https://doi.org/10.1104/pp.113.223941.

Niehaus, A.C., Angilletta, J.M.J., Sears, M.W., Franklin, C.E., Wilson, R.S., 2012. Predicting the physiological performance of ectotherms in fluctuating thermal environments. J. Exp. Biol. 215, 694–701. https://doi.org/10.1242/jeb.058032.

O'Neill, R.V., Goldstein, R.A., Shugart, H.H., Mankin, J.B., 1972. Terrestrial ecosystem energy model. In: East. Deciduous For. Biome Memo Rep. Oak Ridge Environ. Sci. Div. Oak Ridge Natl. Lab.

Padfield, D., Yvon-Durocher, Genevieve, Buckling, A., Jennings, S., Yvon-Durocher, Gabriel, 2015. Rapid evolution of metabolic traits explains thermal adaptation in phytoplankton. Ecol. Lett. 19 https://doi.org/10.1111/ele.12545.

Padfield, D., Lowe, C., Buckling, A., Ffrench-Constant, R., Schaum, E., Jennings, S., Shelley, F., Ólafsson, J.S., Yvon-Durocher, G., 2017. Thermal adaptation constrains the temperature dependence of ecosystem metabolism (preprint). Ecology. https://doi.org/10.1101/108696.

Padfield, D., O'Sullivan, H., Pawar, S., 2021. rTPC and nls.multstart: a new pipeline to fit thermal performance curves in r. Methods Ecol. Evol. 12, 1138–1143. https://doi.org/10.1111/2041-210X.13585.

Patnaik, R., Singh, N.K., Bagchi, S.K., Rao, P.S., Mallick, N., 2019. Utilization of *Scenedesmus obliquus* protein as a replacement of the commercially available fish meal under an algal refinery approach. Front. Microbiol. 10, 2114. https://doi.org/10.3389/fmicb.2019.02114.

Platt, T., Gallegos, C., Harrison, W.G., 1980. Photoinhibition of Photosynthesis in Natural Assemblages of Marine Phytoplankton. Undefined.

Plöhn, M., Spain, O., Sirin, S., Silva, M., Escudero-Oñate, C., Ferrando-Climent, L., Allahverdiyeva, Y., Funk, C., 2021. Wastewater treatment by microalgae. Physiol. Plant. 173, 568–578. https://doi.org/10.1111/ppl.13427.

Ras, M., Steyer, J.-P., Bernard, O., 2013. Temperature effect on microalgae: a crucial factor for outdoor production. Rev. Environ. Sci. Biotechnol. 12, 153–164. https://doi.org/10.1007/s11157-013-9310-6.

Ratkowsky, D.A., Lowry, R.K., McMeekin, T.A., Stokes, A.N., Chandler, R.E., 1983. Model for bacterial culture growth rate throughout the entire biokinetic temperature range. J. Bacteriol. 154, 1222–1226.

Rees, T. a V., Raven, J.A., 2021. The maximum growth rate hypothesis is correct for eukaryotic photosynthetic organisms, but not cyanobacteria. New Phytol. 230, 601–611. https://doi.org/10.1111/nph.17190.

Rezende, E.L., Bozinovic, F., 2019. Thermal performance across levels of biological organization. Philos. Trans. R. Soc. B Biol. Sci. 374, 20180549 https://doi.org/10.1098/rstb.2018.0549.

Schoolfield, R.M., Sharpe, P.J., Magnuson, C.E., 1981. Non-linear regression of biological temperature-dependent rate models based on absolute reaction-rate theory. J. Theor. Biol. 88, 719–731. https://doi.org/10.1016/0022-5193(81)90246-0.

Schulte, P.M., 2015. The effects of temperature on aerobic metabolism: towards a mechanistic understanding of the responses of ectotherms to a changing environment. J. Exp. Biol. 218, 1856–1866. https://doi.org/10.1242/jeb.118851.

Shao, Y., Fang, H., Zhou, H., Wang, Q., Zhu, Y., He, Y., 2017. Detection and imaging of lipids of *Scenedesmus obliquus* based on confocal Raman microspectroscopy. Biotechnol. Biofuels 10, 300. https://doi.org/10.1186/s13068-017-0977-8.

Shekh, A., Sharma, A., Schenk, P.M., Kumar, G., Mudliar, S., 2022. Microalgae cultivation: photobioreactors, CO_2 utilization, and value-added products of industrial importance. J. Chem. Technol. Biotechnol. 97, 1064–1085. https://doi.org/10.1002/jctb.6902.

Slegers, P.M., van Beveren, P.J.M., Wijffels, R.H., van Straten, G., van Boxtel, A.J.B., 2013. Scenario analysis of large scale algae production in tubular photobioreactors. Appl. Energy 105, 395–406. https://doi.org/10.1016/j.apenergy.2012.12.068.

Spain, J.D., 1982. BASIC Microcomputer Models in Biology.

Suga, K., Honjoh, K., Furuya, N., Shimizu, H., Nishi, K., Shinohara, F., Hirabaru, Y., Maruyama, I., Miyamoto, T., Hatano, S., Iio, M., 2002. Two low-temperature-inducible *Chlorella* genes for Δ12 and *ω*-3 fatty acid desaturase (FAD): isolation of Δ12 and ω-3 fad cDNA clones. Biosci. Biotechnol. Biochem. 66, 1314–1327. https://doi.org/10.1271/bbb.66.1314.

Suzuki, H., Hulatt, C.J., Wijffels, R.H., Kiron, V., 2019. Growth and LC-PUFA production of the cold-adapted microalga *Koliella antarctica* in photobioreactors. J. Appl. Phycol. 31 (2), 981–997. https://doi.org/10.1007/s10811-018-1606-z.

Suzuki, H., Détain, A., Park, Y., Viswanath, K., Wijffels, R.H., Leborgne-Castel, N., Procházková, L., Hulatt, C.J., 2023. Phylogeny and lipid profiles of snow-algae isolated from Norwegian red-snow microbiomes. FEMS Microbiol. Ecol. 99 (6), p. fiad057 https://doi.org/10.1093/femsec/fiad057.

Thomas, M.K., Aranguren-Gassis, M., Kremer, C.T., Gould, M.R., Anderson, K., Klausmeier, C.A., Litchman, E., 2017. Temperature–nutrient interactions exacerbate sensitivity to warming in phytoplankton. Glob. Chang. Biol. 23, 3269–3280. https://doi.org/10.1111/gcb.13641.

Ubando, A.T., Anderson, S., Ng, E., Chen, W.-H., Culaba, A.B., Kwon, E.E., 2022. Life cycle assessment of microalgal biorefinery: a state-of-the-art review. Bioresour. Technol. 360, 127615 https://doi.org/10.1016/j.biortech.2022.127615.

Weibull, J.W., 1995. Evolutionary Game Theory. MA, USA, Cambridge.

Wynne, M., Hallan, J., 2015. Reinstatement of Tetradesmus G. M. Smith (Sphaeropleales, Chlorophyta). Feddes Repert, p. 126. https://doi.org/10.1002/fedr.201500021.

Yadav, D., Tanveer, A., Malviya, N., Yadav, S., 2018. Overview and principles of bioengineering: the drivers of omics technologies. In: Barh, D., Azevedo, V., Barh, D., Azevedo, V. (Eds.), Omics Technologies and Bio-engineering, pp. 3–23.

Yvon-Durocher, G., Schaum, C.E., Trimmer, M., 2017. The temperature dependence of phytoplankton stoichiometry: investigating the roles of species sorting and local adaptation. Front. Microbiol. 8, 2003. https://doi.org/10.3389/fmicb.2017.02003.

Zhang, Y., Park, C., Bennett, C., Thornton, M., Kim, D., 2021. Rapid and accurate alignment of nucleotide conversion sequencing reads with HISAT-3N. Genome Res. 31, 1290–1295. https://doi.org/10.1101/gr.275193.120.

Zheng, G., Tian, B., Zhang, F., Tao, F., Li, W., 2011. Plant adaptation to frequent alterations between high and low temperatures: remodelling of membrane lipids and maintenance of unsaturation levels. Plant Cell Environ. 34, 1431–1442. https://doi.org/10.1111/j.1365-3040.2011.02341.x.

Zhou, X.R., Yao, Z.J., Benedicto, K., Nichols, P.D., Green, A., Singh, S., 2023. New sustainable oil seed sources of omega-3 long-chain polyunsaturated fatty acids: a journey from the ocean to the field. Sustain. Basel Switz. 15, 11327. https://doi.org/10.3390/su151411327.